Geophysical Research Letters

RESEARCH LETTER
10.1029/2023GL107733

Anthropogenic Influence on Tropospheric Reactive Bromine Since the Pre-industrial: Implications for Arctic Ice-Core Bromine Trends

Shuting Zhai[1], Joseph R. McConnell[2], Nathan Chellman[2], Michel Legrand[3], Thomas Opel[4], Hanno Meyer[4], Lyatt Jaeglé[1], Kaitlyn Confer[1,5], Koji Fujita[6], Xuan Wang[7], and Becky Alexander[1]

[1]Department of Atmospheric Sciences, University of Washington, Seattle, WA, USA, [2]Division of Hydrologic Sciences, Desert Research Institute, Reno, NV, USA, [3]Université Paris Cité and University Paris Est Creteil, CNRS, LISA, Paris, France, [4]Alfred Wegener Institute Helmholtz Centre for Polar and Marine Research, Potsdam, Germany, [5]Now at Natural Power, Seattle, WA, USA, [6]Graduate School of Environmental Studies, Nagoya University, Nagoya, Japan, [7]School of Energy and Environment, City University of Hong Kong, Kowloon, Hong Kong

Key Points:

- Bromine (Br) concentrations increased 3.5-fold from pre-industrial to 1975 and declined 50% by 1999 in a Russian Arctic ice-core
- A robust correlation between ice-core Br and acidity highlights acidity's key role in influencing the atmospheric Br budget
- Model shows acid-catalyzed sea-salt debromination is the largest source of reactive Br and drives ice-core Br trends

Supporting Information:

Supporting Information may be found in the online version of this article.

Correspondence to:

B. Alexander,
beckya@uw.edu

Citation:

Zhai, S., McConnell, J. R., Chellman, N., Legrand, M., Opel, T., Meyer, H., et al. (2024). Anthropogenic influence on tropospheric reactive bromine since the pre-industrial: Implications for Arctic ice-core bromine trends. *Geophysical Research Letters*, *51*, e2023GL107733. https://doi.org/10.1029/2023GL107733

Received 11 DEC 2023
Accepted 14 FEB 2024

Author Contributions:

Conceptualization: Shuting Zhai, Becky Alexander
Data curation: Shuting Zhai, Joseph R. McConnell, Nathan Chellman, Michel Legrand, Thomas Opel, Hanno Meyer, Lyatt Jaeglé, Kaitlyn Confer, Koji Fujita, Becky Alexander
Formal analysis: Shuting Zhai, Joseph R. McConnell, Nathan Chellman, Thomas Opel, Lyatt Jaeglé, Kaitlyn Confer, Koji Fujita, Becky Alexander

Abstract Tropospheric reactive bromine (Br_y) influences the oxidation capacity of the atmosphere by acting as a sink for ozone and nitrogen oxides. Aerosol acidity plays a crucial role in Br_y abundances through acid-catalyzed debromination from sea-salt-aerosol, the largest global source. Bromine concentrations in a Russian Arctic ice-core, Akademii Nauk, show a 3.5-fold increase from pre-industrial (PI) to the 1970s (peak acidity, PA), and decreased by half to 1999 (present day, PD). Ice-core acidity mirrors this trend, showing robust correlation with bromine, especially after 1940 ($r = 0.9$). Model simulations considering anthropogenic emission changes alone show that atmospheric acidity is the main driver of Br_y changes, consistent with the observed relationship between acidity and bromine. The influence of atmospheric acidity on Br_y should be considered in interpretation of ice-core bromine trends.

Plain Language Summary Reactive bromine in the air impacts major oxidants in our atmosphere, which remove pollutants and greenhouse gases and has changed over time in the Russian Arctic. Ice-core bromine and acidity show a significant increase from pre-industrial to the 1970s followed by a decrease. Our study suggests that human activities caused changes in bromine through the emissions of acidic gases from fossil fuel combustion. Considering relationships between atmospheric acidity and bromine is crucial to interpreting bromine variations in ice cores.

1. Introduction

Tropospheric reactive bromine influences tropospheric oxidation capacity, destroys ozone via catalytic cycles, and perturbs OH to HO_2 ratios toward OH (von Glasow et al., 2004). In coastal polar regions, reactive bromine is responsible for springtime boundary layer ozone depletion events (ODEs) (Barrie et al., 1988; McConnell et al., 1992; Simpson, von Glasow et al., 2007) and gaseous elemental mercury deposition (Steffen et al., 2008; Wang et al., 2019), thus also impacting the transfer of toxic mercury from the atmosphere into the ecosystem.

Natural sources of tropospheric gaseous reactive bromine ($Br_y = Br + HBr + BrNO_2 + BrNO_3 + BrO + HOBr + 2Br_2 + IBr + BrCl$) include sea-salt debromination (Kerkweg et al., 2008; Yang et al., 2005), organobromines emitted from the marine biosphere (Liang et al., 2010; Quack & Wallace, 2003), saline lakes (Hebestreit et al., 1999; Matveev et al., 2001), and volcanoes (Aiuppa et al., 2005; Bobrowski et al., 2003). Anthropogenic sources of Br_y include methyl bromide (CH_3Br) emissions from agricultural pesticide (Clerbaux et al., 2007), coal burning (Lee et al., 2018), biomass burning, and stratospheric transport from halon degradation. Gaseous CH_3Br and aerosol PbBrCl exhaust emissions from leaded gasoline vehicles have been important since the 1920s, but have diminished since the 1970s because of leaded gasoline abatement in North America and Europe (Habibi, 1973; Lammel et al., 2002; Thomas et al., 1997). The 2-fold increase in summertime ice-core bromine after 1950 observed in the Col du Dome ice-core (French Alps) was largely (70%) attributed to leaded gasoline emissions (Legrand et al., 2021b). Global model simulations showed a 39% increase in global Br_y burden from pre-industrial (PI) to present day (PD) driven by enhanced oceanic iodine production from ozone deposition, increased anthropogenic bromocarbons, and increased bromine flux from stratosphere (Sherwen et al., 2017).

Funding acquisition: Joseph R. McConnell, Nathan Chellman, Hanno Meyer, Becky Alexander
Investigation: Shuting Zhai, Joseph R. McConnell, Nathan Chellman, Michel Legrand, Thomas Opel, Hanno Meyer, Koji Fujita, Xuan Wang, Becky Alexander
Methodology: Shuting Zhai, Joseph R. McConnell, Nathan Chellman, Michel Legrand, Thomas Opel, Hanno Meyer, Lyatt Jaeglé, Kaitlyn Confer, Koji Fujita, Xuan Wang, Becky Alexander
Project administration: Joseph R. McConnell, Nathan Chellman, Hanno Meyer, Becky Alexander
Resources: Shuting Zhai, Joseph R. McConnell, Nathan Chellman, Michel Legrand, Lyatt Jaeglé, Kaitlyn Confer, Xuan Wang, Becky Alexander
Software: Shuting Zhai, Koji Fujita, Xuan Wang, Becky Alexander
Supervision: Joseph R. McConnell, Hanno Meyer, Becky Alexander
Validation: Shuting Zhai, Joseph R. McConnell, Nathan Chellman, Michel Legrand, Thomas Opel, Hanno Meyer, Lyatt Jaeglé, Koji Fujita, Becky Alexander
Visualization: Shuting Zhai, Koji Fujita, Becky Alexander
Writing – original draft: Shuting Zhai, Joseph R. McConnell, Becky Alexander
Writing – review & editing: Shuting Zhai, Joseph R. McConnell, Nathan Chellman, Michel Legrand, Thomas Opel, Lyatt Jaeglé, Kaitlyn Confer, Koji Fujita, Xuan Wang, Becky Alexander

However, the model did not consider leaded gasoline or sea-salt debromination, the latter being the largest global source (95%) of Br_y (Wang et al., 2021).

Polar regions have additional sources of Br_y from saline, blowing snow-sourced sea-salt-aerosol (Huang et al., 2020; Savelyev et al., 2006; Yang et al., 2008) and direct snowpack emissions (Abbatt et al., 2012; Foster et al., 2001; Pratt et al., 2013; Simpson, Carlson, et al., 2007, Simpson, von, et al., 2007; Stutz et al., 2011). Both sources are most efficient from snow overlying first-year-sea-ice (FYI), which is thinner, more saline (Confer et al., 2023; Frey et al., 2020; Yang et al., 2008), and contains more snow bromine from upward migration of brine from the sea-ice surface (Nandan et al., 2017; Peterson et al., 2019) than snow over multi-year-sea-ice (MYI). The sea-ice source of Br_y has led to the use of Arctic ice-core bromine as a proxy for historical sea-ice extent (Spolaor et al., 2014, 2016; Sturges & Barrie, 1988; Vallelonga et al., 2021). For example, Spolaor et al. (2016) reported a positive correlation ($r = 0.44$) between bromine excess (Br_{exc}) records from a Russian Arctic ice-core, Akademii Nauk (AN), and spring sea-ice area of the Laptev Sea from 1980 to 1998, with both showing a decreasing trend.

Although total sea-ice extent has been decreasing since at least 1979 (Cavalieri & Parkinson, 2012), FYI has been increasing with the decline of MYI (Bougoudis et al., 2020; Confer et al., 2023). Sea-salt concentrations are observed to increase by 9–12% decade^{-1} during spring and winters in 1980–2017 at Alert, Canada (Confer et al., 2023). Model simulations also show a pan-Arctic increase in surface sea-salt-aerosol concentrations since 1980, mostly due to enhanced blowing snow emissions driven by increased FYI (Confer et al., 2023). With increased FYI in the Arctic since at least 1980, snowpack-emitted bromine may also become a more efficient source (Swanson et al., 2022). Indeed, satellite observations showed increasing trends in tropospheric BrO columns over Arctic sea-ice (+15% decade^{-1}) during polar spring from 1996 to 2017 (Bougoudis et al., 2020).

Although sea-salt release of Br_y is a natural process, the debromination reaction is catalyzed by aerosol acidity (R1–2) (Eigen & Kustin, 1962; Fan & Jacob, 1992), which is influenced by anthropogenic emissions of acidic gases and acidic aerosol precursors such as SO_2 and NO_x(= NO + NO_2).

$$BrNO_3/HOBr(aq) + Br^- (aq) + H^+ (aq) \rightarrow Br_2 + H_2O/HNO_3 (aq) \quad (R1)$$

$$ClNO_3/HOCl(aq) + Br^- (aq) + H^+ (aq) \rightarrow BrCl + H_2O/HNO_3 (aq) \quad (R2)$$

In the Arctic, snow acidity measured in ice cores began increasing in the 1940s, peaked in the 1970s, and decreased to the present day (e.g., Geng et al., 2014). Therefore, the quality of ice-core bromine as a sea-ice proxy may be compromised by these anthropogenic influences (Maselli et al., 2017). The relative impacts of sea-ice extent and atmospheric acidity on bromine trends since PI remain unclear.

Here, we use a global model to quantify the impact of anthropogenic emissions on tropospheric reactive bromine abundances since the pre-industrial. Since previous work suggests that the Russian Arctic AN ice-core preserves an atmospheric signal while Greenland ice cores may not (Zhai et al., 2023), we compare the model to AN ice-core bromine observations. We use the model-ice core comparison to examine implications of anthropogenic emissions for tropospheric Br_y abundance and interpretation of Arctic ice-core bromine records.

2. Methods

2.1. GEOS-Chem Model and Historical Simulations

We use a global 3D chemical transport model GEOS-Chem (version 11-02d, https://github.com/geoschem/geos-chem/tree/v11-02d-prelim) for historical simulations. The model is driven by MERRA-2 assimilated meteorological fields from the Goddard Earth Observing System (GEOS) (Gelaro et al., 2017), and contains detailed HO_x-NO_x-VOC-ozone-halogen-aerosol tropospheric chemistry (Wang et al., 2021) and fully coupled stratospheric chemistry (Eastham et al., 2014). Details of the modeled bromine chemistry are shown in Figures S1–S3 in Supporting Information S1. Sea-salt-aerosol debromination occurs in both open ocean (Jaeglé et al., 2011) and blowing snow (Huang & Jaeglé, 2017) sourced sea-salt-aerosol. Following Zhai et al. (2023), ozone dry deposition velocity onto snow and ice is updated to 0.01 cm s^{-1}, consistent with observations (Simpson, Carlson, et al., 2007, Simpson, von Glasow, et al., 2007). Snowpack bromine emissions (Swanson et al., 2022; Zhai et al., 2023) are not included in the model. The magnitude of the snowpack emission source is estimated to be 278 Gg Br/yr during spring in the AN source regions, based on model simulations from Swanson et al. (2022).

Model simulations are performed under three anthropogenic emission scenarios: pre-industrial (PI, CE 1750), peak atmospheric acidity (PA, CE 1975), and present day (PD, CE 1999). Anthropogenic and biomass burning emissions vary between simulations and are from Community Emissions Data System (CEDS, McDuffie et al., 2020)) and BB4CMIP6 (van Marle et al., 2017), respectively, from individual years (1750, 1975, 1999). The emitted species include but are not limited to acidic precursors, aerosol, organic compounds, methane, and long- and short-lived organohalogens. Details of the emission setup can be found in Zhai et al. (2021), and trends of anthropogenic emissions of SO_2, NO_x, and NH_3 are in Figure S4 in Supporting Information S1. After a 1-yr spin-up, each simulation is run for 1 yr using 2007 meteorology and sea-ice extent. By using the same meteorology, we aim to isolate changes induced by anthropogenic emissions. All simulations are conducted at 4° × 5° horizontal resolution and 72 vertical levels up to 0.01 hPa.

Additionally, the model considered bromine emissions from coal and leaded gasoline consumption. Bromine emissions from coal-fired power plants in the chemical form HBr are expected to be correlated with SO_2 emissions, assuming similar Br:S ratios in coal and the fact that SO_2 control strategies such as wet flue gas desulphurization also remove bromine from exhaust (Lee et al., 2018; McTigue et al., 2014). To calculate coal burning emitted HBr, we scale coal burning emitted SO_2 with a scale factor of Br_x:SO_2 (where $Br_x = BrCl + BrNO_2 + 2\times Br_2) = 1.5 \times 10^{-4}$ ppb:ppb, which is the median of observed Br_x:SO_2 ratios from Lee et al. (2018). This is likely an underestimate since the major form of reactive bromine emitted from coal burning is HBr, which was not measured.

We also added historical emissions of particle-phase PbBrCl and gas-phase CH_3Br from leaded gasoline for PA. Brominated compounds were added to leaded gasoline as additives since 1923 to prevent lead deposition in engines (Thomas et al., 1997). Leaded gasoline phase-out efforts, starting in the 1970s in North America and 1980s in Europe, effectively eliminated global Pb emissions from this source (Hagner, 2002; Huang et al., 1996; Nriagu, 1990). Annual global bromine usage in gasoline peaked in the early 1970s at 170 ± 20 Gg, decreasing to 100 ± 11 Gg in 1980 (Thomas et al., 1997). Assuming complete Br emission into the atmosphere, we estimated global bromine emissions from leaded gasoline in 1975 (average of the early 1970s and 1980, 135 ± 15 Gg) using the transportation-emitted CO and global mean transportation-CO:Br ratio from a global anthropogenic emission inventory, CEDS (McDuffie et al., 2020). Leaded gasoline-sourced bromine is emitted as 85% PbBrCl and 15% CH_3Br based on exhaust measurements (Habibi, 1973; Harsch & Rasmussen, 1977). PbBrCl is modeled as accumulation-mode aerosol, considering the majority of lead particles emitted are <5 μm in wet diameter (Habibi, 1973). Table S1 in Supporting Information S1 shows global and regional total bromine burden from leaded gasoline and coal combustion.

2.2. Ice-Core Bromine and Acidity Observations

A 724 m ice-core was collected from the Akademii Nauk ice cap (80.5ºN, 94.8ºE, 750 m a.s.l.) at Severnaya Zemlya in the Russian Arctic from 1999 to 2001 (Fritzsche et al., 2002; Opel et al., 2013). The snow accumulation rate is about 440 kg m^{-2} yr^{-1}. According to the updated age model, the ice core covers an estimated time range of year 200 BCE–1999 CE (McConnell et al., 2019), but we only present records since CE 1750. This ice core was chosen because it is expected to preserve an atmospheric signal of bromine due to its high snow accumulation rate and high-latitude location, both of which limit photochemical loss of bromine from the snowpack (Zhai et al., 2023).

Total sodium, total bromine, and acidity records from the AN core are previously published (Zhai et al., 2023) and are briefly described here. Elemental sodium (Na) and bromine (Br) were measured continuously with high resolution inductively coupled plasma mass spectrometry (HR-ICP-MS) with an uncertainty of ±10% using the melter-based ice-core analytical system at the Desert Research Institute (Maselli et al., 2017). Mineral acidity (H^+) was measured concurrently using continuous flow analysis (Pasteris et al., 2012), with an uncertainty below 5%. Bromine excess (Br_{exc}) is calculated as shown in Equation 1.

$$[Br_{exc}] = [Br]_{ice-core} - [ssNa]_{ice-core} \times ([Br]/[Na])_{seawater} \quad (1)$$

where [X] is mass concentrations in ng × g ice^{-1}, and $([Br]/[Na])_{sea\ water}$ is the seawater Br/Na mass ratio of 0.00624 (Millero et al., 2008). [ssNa] is calculated based on ice-core calcium concentrations, as described in Maselli et al. (2017).

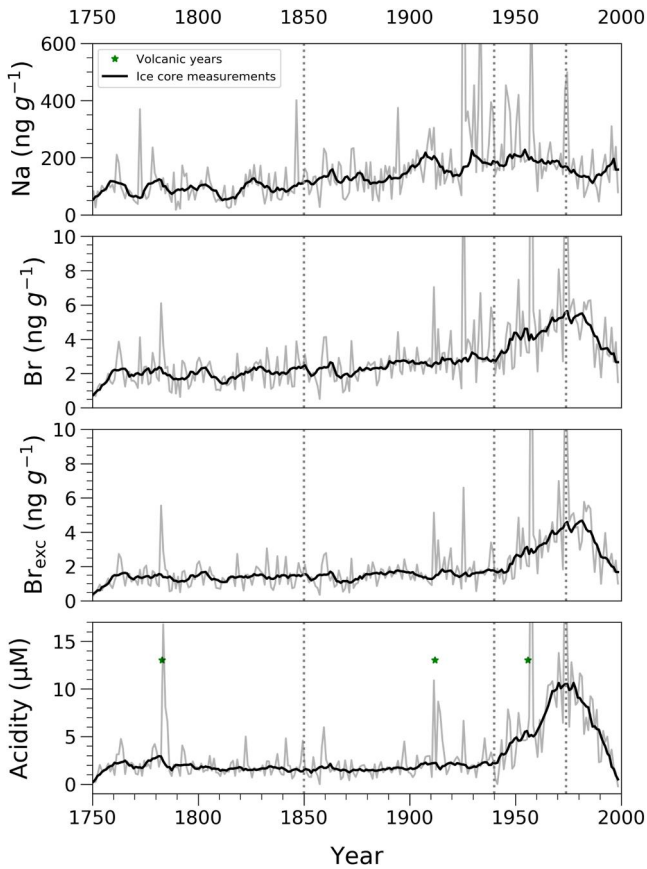

Figure 1. Total sodium, total bromine, Br_{exc}, and acidity concentrations in the Akademii Nauk ice-core. Gray lines are the measured annual ice-core concentrations (total sodium, total bromine, and acidity) or calculations (Br_{exc}), and black lines are the 9-yr running average to reflect long-term variations, with outliers outside of 1.5 × IQR (interquartile range) removed. Green stars mark the large and moderate volcanic years identified in previous study (Opel et al., 2013). Dashed vertical gray lines mark the years 1850, 1940, and 1975.

3. Results

3.1. Ice-Core Bromine Records in the AN Ice-Core

Figure 1 shows total Na, total Br, Br_{exc}, and acidity concentrations in the AN ice core. Change point analysis (Ruggieri, 2013; Zhai et al., 2023) does not identify any change point in the Na record, and there is a slight increasing trend of 0.67 ± 0.00 ng g^{-1} yr^{-1} in Na throughout the record, resulting in a 77% increase from the pre-1850 average Na concentration to that of post-1970. Total Br, Br_{exc}, and acidity show no trends during 1850–1940, and their large increases start in the 1940s. Total Br has an average concentration of 2.02 ± 0.88 ng g^{-1} before 1850, increased by 3.5-fold from pre-1850 to the 1970s, and decreased by 53% after the 1970s to the end of the record (CE 1999). Similar trends are shown in Br_{exc}, with a 4-fold increase from the pre-1850 level to the 1970s, followed by a 59% decrease (Table S2 in Supporting Information S1). Br_{exc}/Br ratio range from 26 to 94%, and are higher (80% ± 6%) in the 1970s compared to PI (1750–1850, 69% ± 11%) and PD (post-1989, 70% ± 11%). Acidity shows a similar trend as Br, with a background concentration of 2.16 ± 1.93 μM before 1850, and an increase of 5.5-fold from pre-1850 to 1975, and decreased by 72% back to PI level by 1999.

Figure 2 shows the relationship between ice-core bromine (Br and Br_{exc}) and acidity. A significant positive correlation ($p < 0.01$) is shown for pre-1850, post-1940, and the full record, with post-1940 showing the highest correlation coefficient ($r = 0.9$). The relationship between ice-core bromine and acidity throughout the record is much stronger than that of bromine and spring sea-ice extent for 1980–1999 reported in Spolaor et al. (2016) ($r = 0.44$), suggesting that it is possible that factors other than sea-ice, such as acidity, may play a role in driving ice-core bromine trends.

3.2. Ice-Core Model Comparison

Figure 3a and Table S3 in Supporting Information S1 show the modeled annual mean tropospheric total bromine burden and its speciation in the AN 5-day back trajectory region (TRJ, Figure S5 in Supporting Information S1) in PI, PA, and PD. Total Br and Br_{exc} are calculated based on Equation 2 and Equation 3, respectively,

$$Br_{total} = Br_y + Br_a^- + Br_c^- \quad (2)$$

$$Br_{exc} = Br_{total} - ssNa \times \left(\frac{[Br]}{[Na]}\right)_{sea\ water} \quad (3)$$

where Br_{total} is total Br, Br_a^- and Br_c^- in Equation 2 are bromide in accumulation-mode and coarse-mode aerosol, respectively, and ssNa sodium in sea-salt-aerosol (both modes).

Modeled Br_y contributes about 95% of total Br in the three time periods, while aerosol bromine is minor (5%); therefore, total Br shows similar distribution and trends as Br_y (Figure S6 in Supporting Information S1). The most abundant Br_y species in PI are Br_2 and BrO, contributing 48% of total Br. Br_2 and BrO burdens remain similar from PI to PA, while HOBr, $BrNO_3$, and BrCl increase by 125%, 392%, and 158%, contributing 24%, 21%, and 11% to total Br in PA, respectively. Increased fractions of $BrNO_3$, HOBr, and BrCl in total Br_y are driven by enhanced NO_x and HO_2 concentrations and more active coupled chlorine-bromine chemistry from PI to PA. Modeled total Br burden and speciation in PD are similar to those of PA. HOBr, $BrNO_2$, and Br_a^- decreased slightly from PA to PD while other species increased.

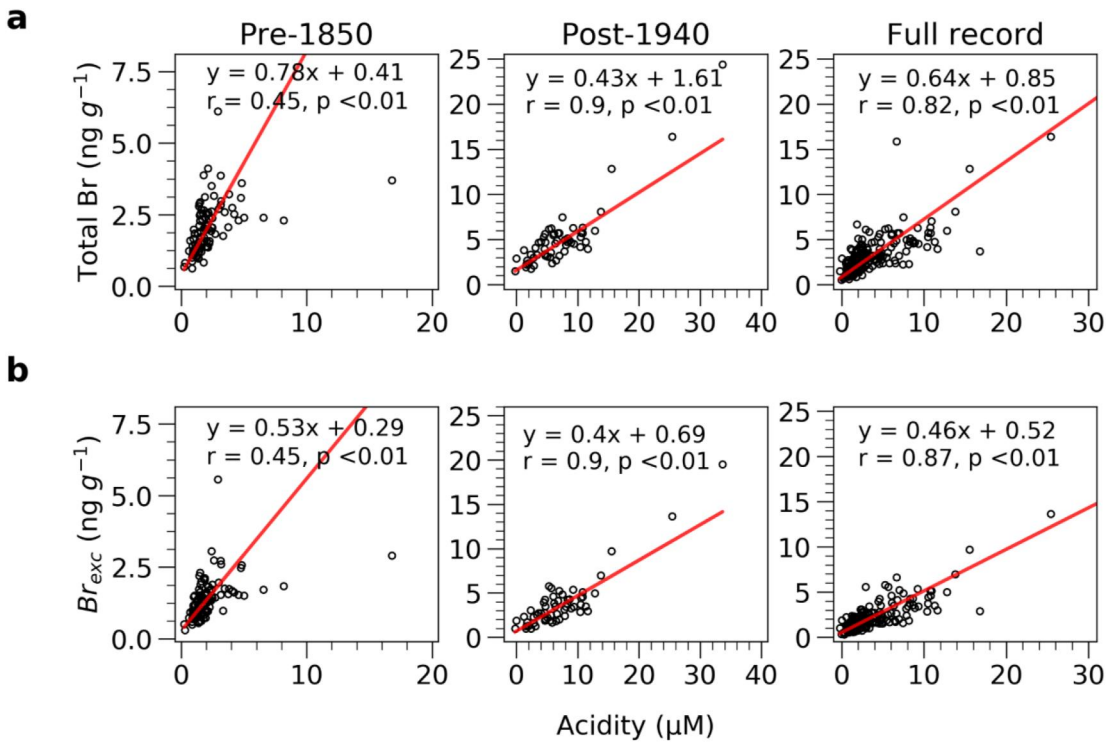

Figure 2. Relationship between concentrations of (a) total Br and acidity, and (b) Br_{exc} and acidity from the AN ice core, for 1750–1850 (pre-1850), 1940–1999 (post-1940), and 1750–1999 (full record). Black circles show the measured Br, Br_{exc}, and acidity concentrations, and red lines represent the reduced major axis regression, with functions shown in each panel.

Br_a^- increased 2.8-fold from PI to PA and decreased 30% from PA to PD (Figures S2 and S3 in Supporting Information S1). In contrast, Br_c^- decreased by 40% from PI to PA and remained low in PD (−0.2% from PA to PD). The opposite trends in Br_a^- and Br_c^- from PI to PA suggest that debromination liberated bromide from coarse-mode aerosol to the gas phase and partially re-partitioned into the accumulation-mode aerosol. Br_{exc}/total Br ratios are 78%, 82%, and 88% for PI, PA, and PD, respectively, consistent with values observed in the AN ice-core (Table S2 in Supporting Information S1).

Figures 3b and 3c compare the percent changes in modeled total bromine and Br_{exc} burdens, respectively, with ice-core total bromine and Br_{exc} concentrations between the 3 time periods. The model predicts a 2-fold increase in total Br and Br_{exc} from PI to PA and only a small decrease (3%) from PA to PD. In comparison, ice-core Br and Br_{exc} show a more symmetrical change centered in 1975 with a 3-fold increase from PI to PA, and 50% decrease from PA to PD. The modeled increase (75% and 96% for total Br and Br_{exc}, respectively) from PI to PD is quantitatively consistent with ice-core observations (64% and 67% for total Br and Br_{exc}, respectively), suggesting that the model may underestimate Br burden in PA (Figure 3b).

3.3. Factors Controlling Modeled Bromine Trends

Figure 4 shows the budget analysis for Br_y, HOBr, $BrNO_3$, and BrCl in the AN TRJ. Sea-salt debromination dominates (>99%) Br_y production in PI, PA, and PD. Organobromines and anthropogenic bromine, including coal combustion and leaded gasoline emissions, contribute less than 1% to the total Br_y sources. Uptake onto sea-salt-aerosol removes >80% of Br_y, while the rest either deposits or is transported out of the TRJ region. Budget analysis shows that HBr uptake on fine-mode-aerosol is the dominant source of Br_a^-, at least one order of magnitude larger than natural emissions from the open ocean and blowing snow on top of sea ice.

Total Br_y production rate increased by 236% from PI to PA. The increase is predominantly driven by enhanced sea-salt-aerosol debromination due to a decrease in aerosol pH from 2.5 to 0.9 in the AN TRJ (Figure S7 in Supporting Information S1). This is consistent with the observed strong correlation ($r = 0.9$, $p < 0.01$) between ice-core Br and acidity after 1940 (Figure 2). From PI to PA, the large increase in Br_y

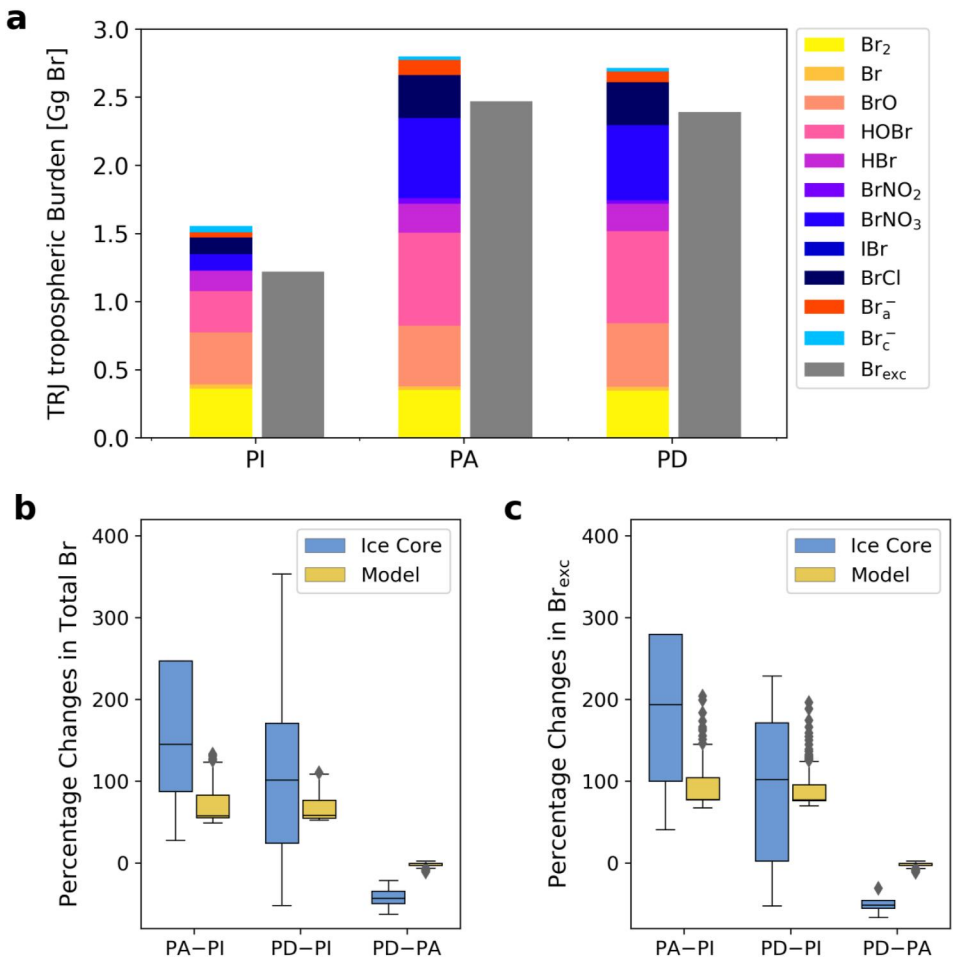

Figure 3. Modeled bromine burden and speciation in the three time periods and model ice-core comparison. (a) Modeled annual mean tropospheric burdens of bromine species (colored bars) and the calculated Br_{exc} burden (gray bars) in the 5-day back trajectory region of AN for PI, PA and PD. Comparison of percentage changes in annual mean tropospheric (b) total Br and (c) Br_{exc} burdens between PI, PA, and PD from AN ice-core records and model simulations. Boxes show the interquartile range (IQR, 25th to 75th percentiles), and the bar in the middle shows the median. Whiskers show 1.5 × IQR range, and data outside of the whiskers are considered outliers.

burden was driven by increases in HOBr, $BrNO_3$, and BrCl. The only source of $BrNO_3$ is the reaction of BrO and NO_2, which increased 3.5-fold caused by enhanced NO_2 (Figure S8 in Supporting Information S1) and BrO abundance (+17%). BrCl production rate increased 1.6-fold, and this is mainly driven by more active halogen recycling on accumulation-mode aerosol ($HOBr + Cl^- + H^+ \rightarrow BrCl + H_2O$), caused both by elevated HOBr burden (Figures S1 and S2 in Supporting Information S1) and more acidic aerosol (Figure S7 in Supporting Information S1). HOBr production rate increased 1.2-fold, caused mainly by increased oxidation of BrO by HO_2, which is driven by enhanced BrO abundance (+17%) and higher HO_2 mixing ratios (+33%) from PI to PA.

From PA to PD, Br_y production rate decreased by 21%, due to reduced aerosol acidity (Figure S7 in Supporting Information S1) and less debromination. Interestingly, modeled Br_y tropospheric burden shows minor changes (Figure 3) because the decrease in Br_y production rate is counterbalanced by a decrease in HBr uptake onto sea-salt-aerosol from PA to PD. This decreasing trend in HBr uptake is driven by the lower tropospheric abundance of HBr (−6%) caused by less formation from the reaction between Br radical and acetaldehyde ($Br + CH_3CHO \rightarrow HBr + CH_3CO$), which is the main source of HBr. In other words, the reduction in tropospheric acetaldehyde burden from PA to PD (−29%), resulting from reduced organic precursors (alkanes and alkenes) emitted from coal combustion and vehicles (McDuffie et al., 2020), causes a decrease in Br_y sinks.

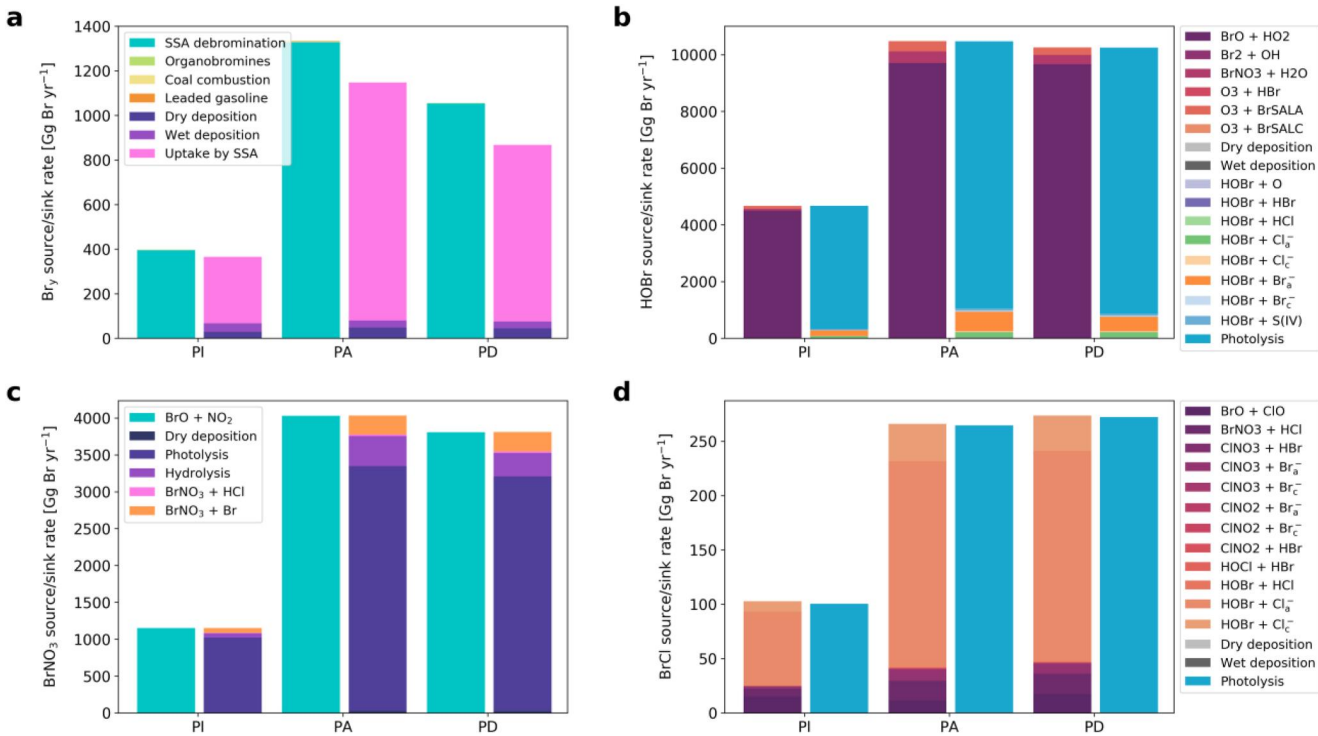

Figure 4. Modeled annual mean sources and sinks of tropospheric (a) Br_y (b) HOBr (c) $BrNO_3$ and (d) BrCl in the AN TRJ for PI, PA, PD. For each time period, left bar shows the sources and right bar shows the sinks. Differences between total sources and total sinks of Br_y can be explained by Br_y that transported outside of the AN TRJ. X_a^-, X_c^- (X = Cl, Br) are chloride and bromide in accumulation- and coarse-mode sea-salt-aerosol, respectively. S(IV) represents SO_3^{2-} and HSO_3^- in cloud droplets.

4. Discussion

The historical simulations with changes in anthropogenic emissions alone can quantitatively capture the AN ice-core bromine changes from PI to PD, but they underestimate the increase in the AN ice-core bromine from PI to PA and do not reproduce the observed −53% decrease in ice-core bromine from PA to PD. No sea-ice changes are simulated, but a model sensitivity study with 1980 meteorology and PA emissions, which has higher total sea-ice extent but lower FYI (−42%) than 2007 (Figure S9 in Supporting Information S1), shows a lower (−6%) tropospheric Br burden due to decreases in blowing snow sourced sea-salt-aerosol (Figure S10 in Supporting Information S1), consistent with the relationship between FYI and blowing snow sourced sea-salt emissions from Confer et al. (2023). The positive relationship between modeled Br_y and FYI is consistent with Bougoudis et al. (2020) and suggests that recent changes in sea ice cannot explain the decline in AN ice-core Br since 1975.

Total bromine measured in the French Alps Col du Dome (CDD) ice-core showed a 2-fold increase in summertime ice-core bromine from the late-1940s to the mid-1970s, followed by a 22% decrease until the end of the record in 2000 (Legrand et al., 2021a). The observed bromine trends were previously interpreted to be driven by leaded gasoline emissions due to the strong correlation between ice-core Br and Pb. Our simulations quantitatively capture the ice-core bromine (Figure S11 in Supporting Information S1) and acidity (Figure S12 in Supporting Information S1) trends. The modeled bromine trends are caused mainly by acid-catalyzed sea-salt debromination, instead of direct emissions from leaded gasoline. Trends in leaded gasoline emissions and anthropogenic acidity are similar.

Acid-catalyzed debromination is the dominant source of Br_y and changes in acidity drive trends in Br_y in the model. The measured acidity in AN ice-core increased 5.5-fold from PI to PA, and decreased back to pre-industrial level in 1999 (Figure 1). However, neither modeled aerosol nor cloud acidity returns to PI levels in PD (Figure S7 in Supporting Information S1). Anthropogenic emissions of acid precursors NO_x and SO_2 in emission inventories declined by 20% and 44%, respectively, from 1975 to 2000 in AN TRJ (Figure S4 in Supporting Information S1), but did not drop back to PI levels. Ammonia emissions declined by 50% (Figure S4 in Supporting Information S1) during the same period, partially counteracting the decrease in SO_2 emissions on

cloud and aerosol pH. The drastic decline in ice-core acidity was not seen in Greenland (Zhai et al., 2023) or Alpine ice-cores (Legrand et al., 2003; Preunkert & Legrand, 2001). The model underestimate in bromine decline from PA to PD is likely due to the underestimated decrease in acidity. The relatively stable modeled Br concentrations from PA to PD is also due to a decline in Br_y loss rate caused by decreased atmospheric acetaldehyde.

The model's limitations also include uncertainties in halogen chemistry, particularly in the HBr/sea-salt Br^- partitioning treated as a kinetic reaction with large uncertainties in GEOS-Chem (Ammann et al., 2013; Wang et al., 2021). This results in a model prediction of bromine depletion for accumulation-mode aerosol in the marine boundary layer, in contrast to observed bromine enrichment (Sander et al., 2003). However, our previous work on ice-core chlorine indicates minimal changes in HCl partitioning from PA to PD (Zhai et al., 2021), suggesting similar stable thermodynamic HBr/sea-salt Br^- partitioning between these periods.

5. Conclusions

Tropospheric reactive bromine destroys surface ozone and has profound impacts on the tropospheric oxidation capacity (Barrie et al., 1988; von Glasow et al., 2004). Both acid-catalyzed debromination (Wang et al., 2021; Zhu et al., 2019) and sea-ice variations (Spolaor et al., 2016; Vallelonga et al., 2021) can influence ice-core bromine trends. However, the relative importance of these factors on Arctic ice-core bromine trends since the pre-industrial remains unclear. We present bromine records since the pre-industrial from the Russian Arctic AN ice-core since PI, and use GEOS-Chem model simulations to examine the trends. The AN ice core shows a 3.5-fold increase in total Br from pre-1850 to the 1970s, followed by a 53% decrease from the 1970s to 1999. Measured ice-core acidity increased by a factor of 5.5, followed by a 72% decrease after the 1970s and a return to PI levels by the end of the record. Ice-core bromine and acidity are strongly correlated, particularly after 1940 ($r = 0.9$).

The model suggests that sea-salt debromination is the dominant (>99%) source of Br_y in all emission scenarios, and direct emissions of anthropogenic bromine contribute less than 1% to the total Br_y sources. Modeled changes in anthropogenic acidity alone can explain the 64–67% increase in Br and Br_{exc} observed in the AN ice-core between PI and PD. The modeled 2-fold increase in Br_y is smaller than the observed increase in ice-core Br_{exc} (3-fold) from pre-1850 to 1975, and the modeled increase is driven by increases in anthropogenic emissions of acid gas precursors. The modeled relationship between atmospheric Br_y and acidity is consistent with observed relationships between ice-core bromine and acidity from AN (Figure 2) and a mid-latitude alpine ice-core (Legrand et al., 2021a).

The model does not capture the observed decrease in both Br_y (53%) and acidity (72%) after 1975, possibly because of uncertainties in anthropogenic emissions and transport of acidic gas-phase precursors. Since variability in atmospheric Br_y is driven by atmospheric acidity, the modeled underestimate of the decline in acidity since 1975 contributes to the modeled underestimate of the decline in Br_{exc}. Our results suggest that anthropogenic acidity has had a profound influence on the production and abundance of tropospheric reactive bromine (Br_y), with implications for the oxidation capacity of the atmosphere. The use of ice-core bromine as a proxy for past changes in sea-ice extent must consider changes in atmospheric acidity in the interpretation of observed trends, especially when ice-core acidity changes.

Data Availability Statement

Ice-core data for this research can be downloaded from the Arctic Data Center with Creative Commons Attribution (McConnell, 2023). GEOS-Chem is open software and available for download (Yantosca et al., 2021). GEOS-Chem historical simulations output is archived in the Dryad Data Repository (Zhai & Alexander, 2023).

Acknowledgments
Becky Alexander and Shuting Zhai acknowledge support from U.S. National Science Foundation (NSF) grants AGS 2202287 and 1702266. For the ice-core data, Joseph R. McConnell acknowledges support from NSF grants 0909541, 1023672, 1204176, and 1702830, and Nathan Chellman acknowledges support from NSF Grant 2102917. The authors also thank the Alfred Wegener Institute, the U. S. Ice Drilling Program, as well as staff and students of the DRI ice-core laboratory including O. Maselli, D. Pasteris, and L. Layman.

References

Abbatt, J. P. D., Thomas, J. L., Abrahamsson, K., Boxe, C., Granfors, A., Jones, A. E., et al. (2012). Halogen activation via interactions with environmental ice and snow in the polar lower troposphere and other regions. *Atmospheric Chemistry and Physics*, *12*(14), 6237–6271. https://doi.org/10.5194/acp-12-6237-2012

Aiuppa, A., Federico, C., Franco, A., Giudice, G., Gurrieri, S., Inguaggiato, S., et al. (2005). Emission of bromine and iodine from Mount Etna volcano. *Geochemistry, Geophysics, Geosystems*, *6*(8). https://doi.org/10.1029/2005gc000965

Ammann, M., Cox, R. A., Crowley, J. N., Jenkin, M. E., Mellouki, A., Rossi, M. J., et al. (2013). Evaluated kinetic and photochemical data for atmospheric chemistry: Volume VI – Heterogeneous reactions with liquid substrates. *Atmospheric Chemistry and Physics*, *13*(16), 8045–8228. https://doi.org/10.5194/acp-13-8045-2013

Barrie, L. A., Bottenheim, J. W., Schnell, R. C., Crutzen, P. J., & Rasmussen, R. A. (1988). Ozone destruction and photochemical reactions at polar sunrise in the lower Arctic atmosphere. *Nature*, *334*(6178), 138–141. https://doi.org/10.1038/334138a0

Bobrowski, N., Hönninger, G., Galle, B., & Platt, U. (2003). Detection of bromine monoxide in a volcanic plume. *Nature*, *423*(6937), 273–276. https://doi.org/10.1038/nature01625

Bougoudis, I., Blechschmidt, A.-M., Richter, A., Seo, S., Burrows, J. P., Theys, N., & Rinke, A. (2020). Long-term time series of Arctic tropospheric BrO derived from UV–VIS satellite remote sensing and its relation to first-year sea ice. *Atmospheric Chemistry and Physics*, *20*(20), 11869–11892. https://doi.org/10.5194/acp-20-11869-2020

Cavalieri, D. J., & Parkinson, C. L. (2012). Arctic sea ice variability and trends, 1979–2010. *The Cryosphere*, *6*(4), 881–889. https://doi.org/10.5194/tc-6-881-2012

Clerbaux, C., Cunnold, D. M., Anderson, J., Engel, A., Fraser, P. J., Mahieu, E., et al. (2007). Scientific assessment of ozone depletion: 2006. In *Global Ozone Research and Monitoring Project - Report No. 50*. Retrieved from https://agris.fao.org/agris-search/search.do?recordID=BE2014102317

Confer, K. L., Jaeglé, L., Liston, G. E., Sharma, S., Nandan, V., Yackel, J., et al. (2023). Impact of changing Arctic sea ice extent, sea ice age, and snow depth on sea salt aerosol from blowing snow and the open ocean for 1980–2017. *Journal of Geophysical Research*, *128*(3). https://doi.org/10.1029/2022jd037667

Eastham, S. D., Weisenstein, D. K., & Barrett, S. R. H. (2014). Development and evaluation of the unified tropospheric–stratospheric chemistry extension (UCX) for the global chemistry-transport model GEOS-Chem. *Atmospheric Environment*, *89*, 52–63. https://doi.org/10.1016/j.atmosenv.2014.02.001

Eigen, M., & Kustin, K. (1962). The kinetics of halogen hydrolysis. *Journal of the American Chemical Society*, *84*(8), 1355–1361. https://doi.org/10.1021/ja00867a005

Fan, S.-M., & Jacob, D. J. (1992). Surface ozone depletion in Arctic spring sustained by bromine reactions on aerosols. *Nature*, *359*(6395), 522–524. https://doi.org/10.1038/359522a0

Foster, K. L., Plastridge, R. A., Bottenheim, J. W., Shepson, P. B., Finlayson-Pitts, B. J., & Spicer, C. W. (2001). The role of Br2 and BrCl in surface ozone destruction at polar sunrise. *Science*, *291*(5503), 471–474. https://doi.org/10.1126/science.291.5503.471

Frey, M. M., Norris, S. J., Brooks, I. M., Anderson, P. S., Nishimura, K., Yang, X., et al. (2020). First direct observation of sea salt aerosol production from blowing snow above sea ice. *Atmospheric Chemistry and Physics*, *20*(4), 2549–2578. https://doi.org/10.5194/acp-20-2549-2020

Fritzsche, D., Wilhelms, F., Savatyugin, L. M., Pinglot, J. F., Meyer, H., Hubberten, H.-W., & Miller, H. (2002). A new deep ice core from Akademii Nauk ice cap, Severnaya Zemlya, Eurasian Arctic: First results. *Annals of Glaciology*, *35*, 25–28. https://doi.org/10.3189/172756402781816645

Gelaro, R., McCarty, W., Suárez, M. J., Todling, R., Molod, A., Takacs, L., et al. (2017). The Modern-Era Retrospective Analysis for Research and Applications, Version 2 (MERRA-2). *Journal of Climate*, *30*(13), 5419–5454. https://doi.org/10.1175/JCLI-D-16-0758.1

Geng, L., Alexander, B., Cole-Dai, J., Steig, E. J., Savarino, J., Sofen, E. D., & Schauer, A. J. (2014). Nitrogen isotopes in ice core nitrate linked to anthropogenic atmospheric acidity change. *Proceedings of the National Academy of Sciences of the United States of America*, *111*(16), 5808–5812. https://doi.org/10.1073/pnas.1319441111

Habibi, K. (1973). Characterization of particulate matter in vehicle exhaust. *Environmental Science and Technology*, *7*(3), 223–234. https://doi.org/10.1021/es60075a001

Hagner, C. (2002). Regional and long-term patterns of lead concentrations in riverine, marine and terrestrial systems and humans in Northwest Europe. *Water, Air, and Soil Pollution*, *134*(1/4), 1–40. https://doi.org/10.1023/a:1014191519871

Harsch, D. E., & Rasmussen, R. A. (1977). Identification of methyl bromide in urban air. *Analytical Letters*, *10*(13), 1041–1047. https://doi.org/10.1080/00032717708067841

Hebestreit, K., Stutz, J., Rosen, D., Matveiv, V., Peleg, M., Luria, M., & Platt, U. (1999). DOAS measurements of tropospheric bromine oxide in mid-latitudes. *Science*, *283*(5398), 55–57. https://doi.org/10.1126/science.283.5398.55

Huang, J., & Jaeglé, L. (2017). Wintertime enhancements of sea salt aerosol in polar regions consistent with a sea ice source from blowing snow. *Atmospheric Chemistry and Physics*, *17*(5), 3699–3712. https://doi.org/10.5194/acp-17-3699-2017

Huang, J., Jaeglé, L., Chen, Q., Alexander, B., Sherwen, T., Evans, M. J., et al. (2020). Evaluating the impact of blowing-snow sea salt aerosol on springtime BrO and O_3 in the Arctic. *Atmospheric Chemistry and Physics*, *20*(12), 7335–7358. https://doi.org/10.5194/acp-20-7335-2020

Huang, S., Arimoto, R., & Rahn, K. A. (1996). Changes in atmospheric lead and other pollution elements at Bermuda. *Journal of Geophysical Research*, *101*(D15), 21033–21040. https://doi.org/10.1029/96jd02001

Jaeglé, L., Quinn, P. K., Bates, T. S., Alexander, B., & Lin, J.-T. (2011). Global distribution of sea salt aerosols: New constraints from in situ and remote sensing observations. *Atmospheric Chemistry and Physics*, *11*(7), 3137–3157. https://doi.org/10.5194/acp-11-3137-2011

Kerkweg, A., Jöckel, P., Pozzer, A., Tost, H., Sander, R., Schulz, M., et al. (2008). Consistent simulation of bromine chemistry from the marine boundary layer to the stratosphere – Part 1: Model description, sea salt aerosols and pH. *Atmospheric Chemistry and Physics*, *8*(19), 5899–5917. https://doi.org/10.5194/acp-8-5899-2008

Lammel, G., Röhrl, A., & Schreiber, H. (2002). Atmospheric lead and bromine in Germany. *Environmental Science and Pollution Research*, *9*(6), 397–404. https://doi.org/10.1007/BF02987589

Lee, B. H., Lopez-Hilfiker, F. D., Schroder, J. C., Campuzano-Jost, P., Jimenez, J. L., McDuffie, E. E., et al. (2018). Airborne observations of reactive inorganic chlorine and bromine species in the exhaust of coal-fired power plants. *Journal of Geophysical Research, D: Atmospheres*, *123*(19), 11225–11237. https://doi.org/10.1029/2018JD029284

Legrand, M., McConnell, J. R., Preunkert, S., Chellman, N. J., & Arienzo, M. (2021a). Causes of enhanced bromine levels in Alpine ice cores during the 20th century: Implications for bromine in the free European troposphere. *Journal of Geophysical Research*, *126*(8). https://doi.org/10.1029/2020jd034246

Legrand, M., McConnell, J. R., Preunkert, S., Chellman, N. J., & Arienzo, M. M. (2021b). Causes of enhanced bromine levels in alpine ice cores during the 20th century: Implications for bromine in the free European troposphere. *Journal of Geophysical Research*, *126*(8). https://doi.org/10.1029/2020jd034246

Legrand, M., Preunkert, S., Wagenbach, D., Cachier, H., & Puxbaum, H. (2003). A historical record of formate and acetate from a high-elevation Alpine glacier: Implications for their natural versus anthropogenic budgets at the European scale. *Journal of Geophysical Research*, *108*(D24). https://doi.org/10.1029/2003jd003594

Liang, Q., Stolarski, R. S., Kawa, S. R., Nielsen, J. E., Douglass, A. R., Rodriguez, J. M., et al. (2010). Finding the missing stratospheric Br_y: A global modeling study of $CHBr_3$ and CH_2Br_2. *Atmospheric Chemistry and Physics*, *10*(5), 2269–2286. https://doi.org/10.5194/acp-10-2269-2010

Maselli, O. J., Chellman, N. J., Grieman, M., Layman, L., McConnell, J. R., Pasteris, D., et al. (2017). Sea ice and pollution-modulated changes in Greenland ice core methanesulfonate and bromine. *Climate of the Past*, *13*(1), 39–59. https://doi.org/10.5194/cp-13-39-2017

Matveev, V., Peleg, M., Rosen, D., Tov-Alper, D. S., Hebestreit, K., Stutz, J., et al. (2001). Bromine oxide-ozone interaction over the Dead Sea. *Journal of Geophysical Research*, *106*(D10), 10375–10387. https://doi.org/10.1029/2000jd900611

McConnell, J. C. (2023). Acidity, sodium, and bromine concentrations from the Akademii Nauk (AN), ACT_11d, Summit10 (Summit), Tunu, NGT_B19, and NEEM_2011_S1 ice cores, drilled 1993-2011 [Dataset]. Arctic Data Center. https://doi.org/10.18739/A2K649V3D

McConnell, J. C., Henderson, G. S., Barrie, L., Bottenheim, J., Niki, H., Langford, C. H., & Templeton, E. M. J. (1992). Photochemical bromine production implicated in Arctic boundary-layer ozone depletion. *Nature*, *355*(6356), 150–152. https://doi.org/10.1038/355150a0

McConnell, J. R., Chellman, N. J., Wilson, A. I., Stohl, A., Arienzo, M. M., Eckhardt, S., et al. (2019). Pervasive Arctic lead pollution suggests substantial growth in medieval silver production modulated by plague, climate, and conflict. *Proceedings of the National Academy of Sciences of the United States of America*, *116*(30), 14910–14915. https://doi.org/10.1073/pnas.1904515116

McDuffie, E. E., Smith, S. J., O'Rourke, P., Tibrewal, K., Venkataraman, C., Marais, E. A., et al. (2020). A global anthropogenic emission inventory of atmospheric pollutants from sector- and fuel-specific sources (1970–2017): An application of the Community Emissions Data System (CEDS). *Earth System Science Data*, *12*(4), 3413–3442. https://doi.org/10.5194/essd-12-3413-2020

McTigue, N. E., Cornwell, D. A., Graf, K., & Brown, R. (2014). Occurrence and consequences of increased bromide in drinking water sources. *Journal - American Water Works Association*, *106*(11), E492–E508. https://doi.org/10.5942/jawwa.2014.106.0141

Millero, F. J., Feistel, R., Wright, D. G., & McDougall, T. J. (2008). The composition of standard seawater and the definition of the reference-composition salinity scale. *Deep Sea Research Part I: Oceanographic Research Papers*, *55*(1), 50–72. https://doi.org/10.1016/j.dsr.2007.10.001

Nandan, V., Geldsetzer, T., Yackel, J., Mahmud, M., Scharien, R., Howell, S., et al. (2017). Effect of snow salinity on CryoSat-2 Arctic first-year sea ice freeboard measurements. *Geophysical Research Letters*, *44*(20), 10419–10426. https://doi.org/10.1002/2017gl074506

Nriagu, J. O. (1990). The rise and fall of leaded gasoline. *The Science of the Total Environment*, *92*, 13–28. https://doi.org/10.1016/0048-9697(90)90318-O

Opel, T., Fritzsche, D., & Meyer, H. (2013). Eurasian Arctic climate over the past millennium as recorded in the Akademii Nauk ice core (Severnaya Zemlya). *Climate of the Past*, *9*(5), 2379–2389. https://doi.org/10.5194/cp-9-2379-2013

Pasteris, D. R., McConnell, J. R., & Edwards, R. (2012). High-resolution, continuous method for measurement of acidity in ice cores. *Environmental Science and Technology*, *46*(3), 1659–1666. https://doi.org/10.1021/es202668n

Peterson, P. K., Hartwig, M., May, N. W., Schwartz, E., Rigor, I., Ermold, W., et al. (2019). Snowpack measurements suggest role for multi-year sea ice regions in Arctic atmospheric bromine and chlorine chemistry. *Elem Sci Anth*, *7*(1), 14. https://doi.org/10.1525/elementa.352

Pratt, K. A., Custard, K. D., Shepson, P. B., Douglas, T. A., Pöhler, D., General, S., et al. (2013). Photochemical production of molecular bromine in Arctic surface snowpacks. *Nature Geoscience*, *6*(5), 351–356. https://doi.org/10.1038/ngeo1779

Preunkert, S., Legrand, M., & Wagenbach, D. (2001). Sulfate trends in a Col du Dome (French Alps) ice core: A record of anthropogenic sulfate levels in the European midtroposphere over the twentieth century. *Journal of Geophysical Research*, *106*(D23), 31991–32004. https://doi.org/10.1029/2001JD000792

Quack, B., & Wallace, D. W. R. (2003). Air-sea flux of bromoform: Controls, rates, and implications. *Global Biogeochemical Cycles*, *17*(1). https://doi.org/10.1029/2002gb001890

Ruggieri, E. (2013). A Bayesian approach to detecting change points in climatic records. *International Journal of Climatology*, *33*(2), 520–528. https://doi.org/10.1002/joc.3447

Sander, R., Keene, W. C., Pszenny, A. A. P., Arimoto, R., Ayers, G. P., Baboukas, E., et al. (2003). Inorganic bromine in the marine boundary layer: A critical review. *Atmospheric*, *3*(5), 1301–1336. https://doi.org/10.5194/acp-3-1301-2003

Savelyev, S. A., Gordon, M., Hanesiak, J., Papakyriakou, T., & Taylor, P. A. (2006). Blowing snow studies in the Canadian Arctic Shelf Exchange Study, 2003–04. *Hydrological Processes*, *20*(4), 817–827. https://doi.org/10.1002/hyp.6118

Sherwen, T., Evans, M. J., Carpenter, L. J., Schmidt, J. A., & Mickley, L. J. (2017). Halogen chemistry reduces tropospheric O_3 radiative forcing. *Atmospheric Chemistry and Physics*, *17*(2), 1557–1569. https://doi.org/10.5194/acp-17-1557-2017

Simpson, W. R., Carlson, D., Hönninger, G., Douglas, T. A., Sturm, M., Perovich, D., et al. (2007). First-year sea-ice contact predicts bromine monoxide (BrO) levels at Barrow, Alaska better than potential frost flower contact. *Atmospheric Chemistry and Physics*, *7*(3), 621–627. https://doi.org/10.5194/acp-7-621-2007

Simpson, W. R., von Glasow, R., Riedel, K., Anderson, P., Ariya, P., Bottenheim, J., et al. (2007). Halogens and their role in polar boundary-layer ozone depletion. *Atmospheric Chemistry and Physics Discussions: ACPD*, *7*(2), 4285–4403. https://doi.org/10.5194/acpd-7-4285-2007

Spolaor, A., Opel, T., McConnell, J. R., Maselli, O. J., Spreen, G., Varin, C., et al. (2016). Halogen-based reconstruction of Russian Arctic sea ice area from the Akademii Nauk ice core (Severnaya Zemlya). *The Cryosphere*, *10*(1), 245–256. https://doi.org/10.5194/tc-10-245-2016

Spolaor, A., Vallelonga, P., Gabrieli, J., Martma, T., Björkman, M. P., Isaksson, E., et al. (2014). Seasonality of halogen deposition in polar snow and ice. *Atmospheric Chemistry and Physics*, *14*(18), 9613–9622. https://doi.org/10.5194/acp-14-9613-2014

Steffen, A., Douglas, T., Amyot, M., Ariya, P., Aspmo, K., Berg, T., et al. (2008). A synthesis of atmospheric mercury depletion event chemistry in the atmosphere and snow. *Atmospheric*, *8*(6), 1445–1482. https://doi.org/10.5194/acp-8-1445-2008

Sturges, W. T., & Barrie, L. A. (1988). Chlorine, bromine AND iodine in Arctic aerosols. *Atmospheric Environment*, *22*(6), 1179–1194. https://doi.org/10.1016/0004-6981(88)90349-6

Stutz, J., Thomas, J. L., Hurlock, S. C., Schneider, M., von Glasow, R., Piot, M., et al. (2011). Longpath DOAS observations of surface BrO at Summit, Greenland. *Atmospheric Chemistry and Physics*, *11*(18), 9899–9910. https://doi.org/10.5194/acp-11-9899-2011

Swanson, W. F., Holmes, C. D., Simpson, W. R., Confer, K., Marelle, L., Thomas, J. L., et al. (2022). Comparison of model and ground observations finds snowpack and blowing snow aerosols both contribute to Arctic tropospheric reactive bromine. *Atmospheric Chemistry and Physics*, *22*(22), 14467–14488. https://doi.org/10.5194/acp-22-14467-2022

Thomas, V. M., Bedford, J. A., & Cicerone, R. J. (1997). Bromine emissions from leaded gasoline. *Geophysical Research Letters*, *24*(11), 1371–1374. https://doi.org/10.1029/97gl01243

Vallelonga, P., Maffezzoli, N., Saiz-Lopez, A., Scoto, F., Kjær, H. A., & Spolaor, A. (2021). Sea-ice reconstructions from bromine and iodine in ice cores. *Quaternary Science Reviews*, *269*, 107133. https://doi.org/10.1016/j.quascirev.2021.107133

van Marle, M. J. E., Kloster, S., Magi, B. I., Marlon, J. R., Daniau, A.-L., Field, R. D., et al. (2017). Historic global biomass burning emissions for CMIP6 (BB4CMIP) based on merging satellite observations with proxies and fire models (1750–2015). *Geoscientific Model Development*, *10*(9), 3329–3357. https://doi.org/10.5194/gmd-10-3329-2017

von Glasow, R., von Kuhlmann, R., Lawrence, M. G., Platt, U., & Crutzen, P. J. (2004). Impact of reactive bromine chemistry in the troposphere. *Atmospheric Chemistry and Physics*, *4*(11/12), 2481–2497. https://doi.org/10.5194/acp-4-2481-2004

Wang, S., McNamara, S. M., Moore, C. W., Obrist, D., Steffen, A., Shepson, P. B., et al. (2019). Direct detection of atmospheric atomic bromine leading to mercury and ozone depletion. *Proceedings of the National Academy of Sciences of the United States of America*, *116*(29), 14479–14484. https://doi.org/10.1073/pnas.1900613116

Wang, X., Jacob, D. J., Downs, W., Zhai, S., Zhu, L., Shah, V., et al. (2021). Global tropospheric halogen (Cl, Br, I) chemistry and its impact on oxidants. https://doi.org/10.5194/acp-2021-441

Yang, X., Cox, R. A., Warwick, N. J., Pyle, J. A., Carver, G. D., O'Connor, F. M., & Savage, N. H. (2005). Tropospheric bromine chemistry and its impacts on ozone: A model study. *Journal of Geophysical Research*, *110*(D23), 3719. https://doi.org/10.1029/2005JD006244

Yang, X., Pyle, J. A., & Cox, R. A. (2008). Sea salt aerosol production and bromine release: Role of snow on sea ice. *Geophysical Research Letters*, *35*(16). https://doi.org/10.1029/2008gl034536

Yantosca, B., Sulprizio, M., Lundgren, L., kelvinhb, 22degrees, Ridley, D., et al. (2021). GEOS-Chem Version v11-02d-prelim-zenodo [Software]. Zenodo. Retrieved from https://zenodo.org/records/5047976

Zhai, S., & Alexander, B. (2023). Data to support: Anthropogenic influence on tropospheric reactive bromine since the pre-industrial: Implications for ice-core bromine trends [Dataset]. Dryad. https://doi.org/10.5061/dryad.pk0p2ngw5

Zhai, S., Swanson, W., McConnell, J. R., Chellman, N., Opel, T., Sigl, M., et al. (2023). Implications of snowpack reactive bromine production for Arctic ice core bromine preservation. *Journal of Geophysical Research*, *128*(20). https://doi.org/10.1029/2023jd039257

Zhai, S., Wang, X., McConnell, J. R., Geng, L., Cole-Dai, J., Sigl, M., et al. (2021). Anthropogenic impacts on tropospheric reactive chlorine since the preindustrial. *Geophysical Research Letters*, *48*(14). https://doi.org/10.1029/2021gl093808

Zhu, L., Jacob, D. J., Eastham, S. D., Sulprizio, M. P., Wang, X., Sherwen, T., et al. (2019). Effect of sea salt aerosol on tropospheric bromine chemistry. *Atmospheric Chemistry and Physics*, *19*(9), 6497–6507. https://doi.org/10.5194/acp-19-6497-2019

Geophysical Research Letters

Supporting Information for

Anthropogenic influence on tropospheric reactive bromine since the pre-industrial: Implications for ice-core bromine trends

Shuting Zhai[1], Joseph R. McConnell[2], Nathan Chellman[2], Michel Legrand[3], Thomas Opel[4], Hanno Meyer[4], Lyatt Jaeglé[1], Kaitlyn Confer[1†], Koji Fujita[5], Xuan Wang[6], Becky Alexander[1]

[1]Department of Atmospheric Sciences, University of Washington, Seattle, Washington, US.

[2]Division of Hydrologic Sciences, Desert Research Institute, Reno, NV, US.

[3]LISA (Laboratoire Interuniversitaire des Systèmes Atmosphériques), UMR CNRS 7583, Université Paris-Est-Créteil, Université de Paris, Institut Pierre Simon Laplace, Créteil, France

[4]Alfred Wegener Institute Helmholtz Centre for Polar and Marine Research, Potsdam, Germany

[5]Graduate School of Environmental Studies, Nagoya University, Nagoya, Japan.

[6]School of Energy and Environment, City University of Hong Kong, Hong Kong SAR, China

Now at:

† Natural Power, Seattle, Washington, United States

Corresponding author: Becky Alexander (beckya@uw.edu)

Contents of this file

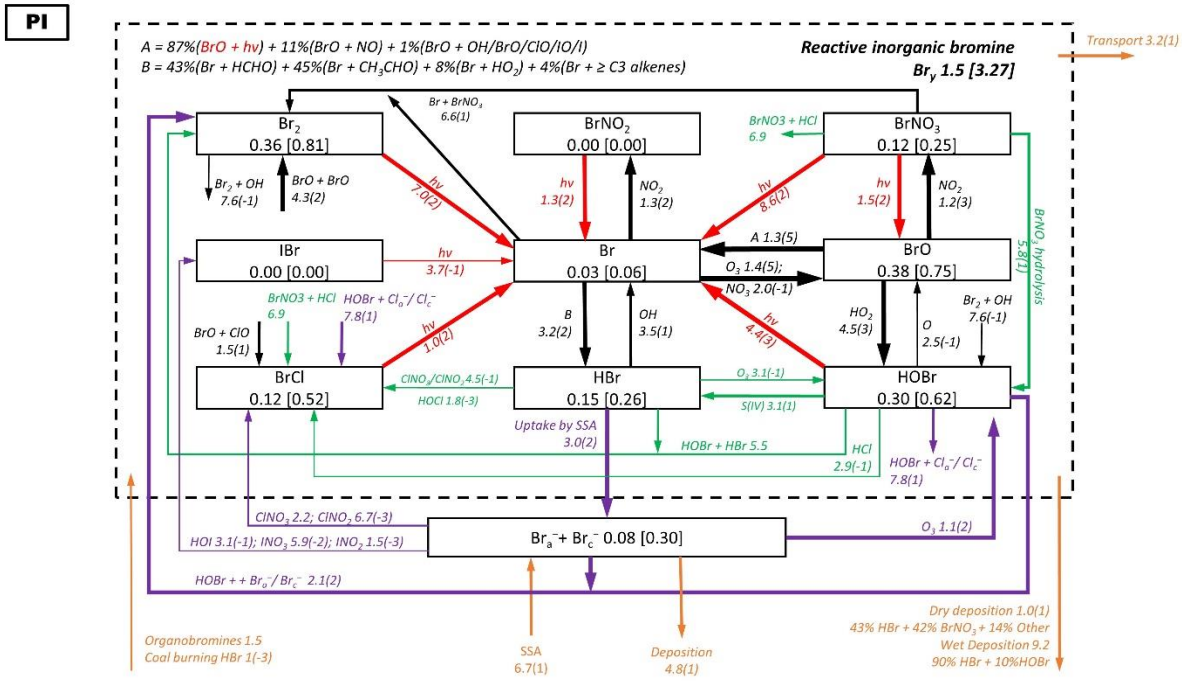

Figure S1. AN TRJ regional budget and chemical cycling of tropospheric bromine species in GEOS-Chem for PI. Average regional annual mean masses (Gg Br) and mixing ratios (ppt, in square brackets) are shown in the squares with key bromine species. Arrows show the regional annual mean reaction rates (Gg Br a^{-1}), and the thickness of arrows are proportional to the orders of magnitude of the reaction rates. Read 8.6(2) as 8.6×10^2. Gas phase, aerosol multi-phase, cloud, and photolysis chemistry are shown in black, purple, green, and red arrows, respectively, and orange arrows indicate the sources and sinks. The dotted box group together the Br_y family, and arrows in and out of the box represent general sources and sinks of Br_y. Cl_a^- and Cl_c^- represent chloride in accumulation-mode and coarse-mode sea-salt aerosol, respectively.

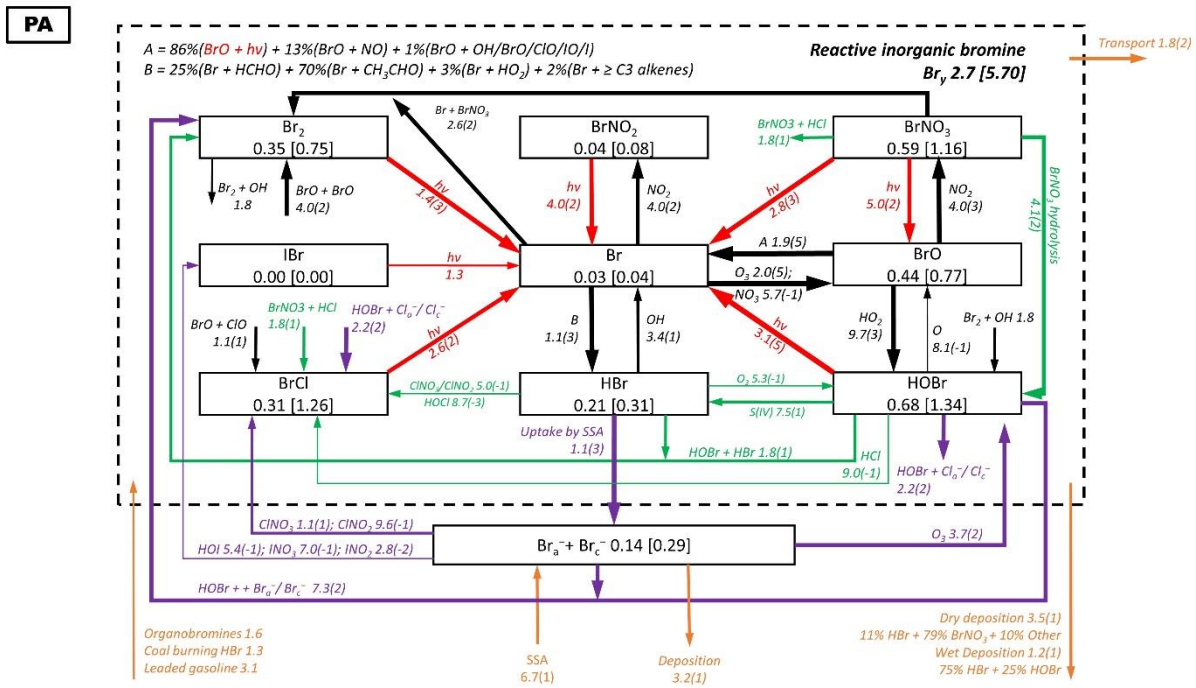

Figure S2. Similar to Figure S1 but for PA.

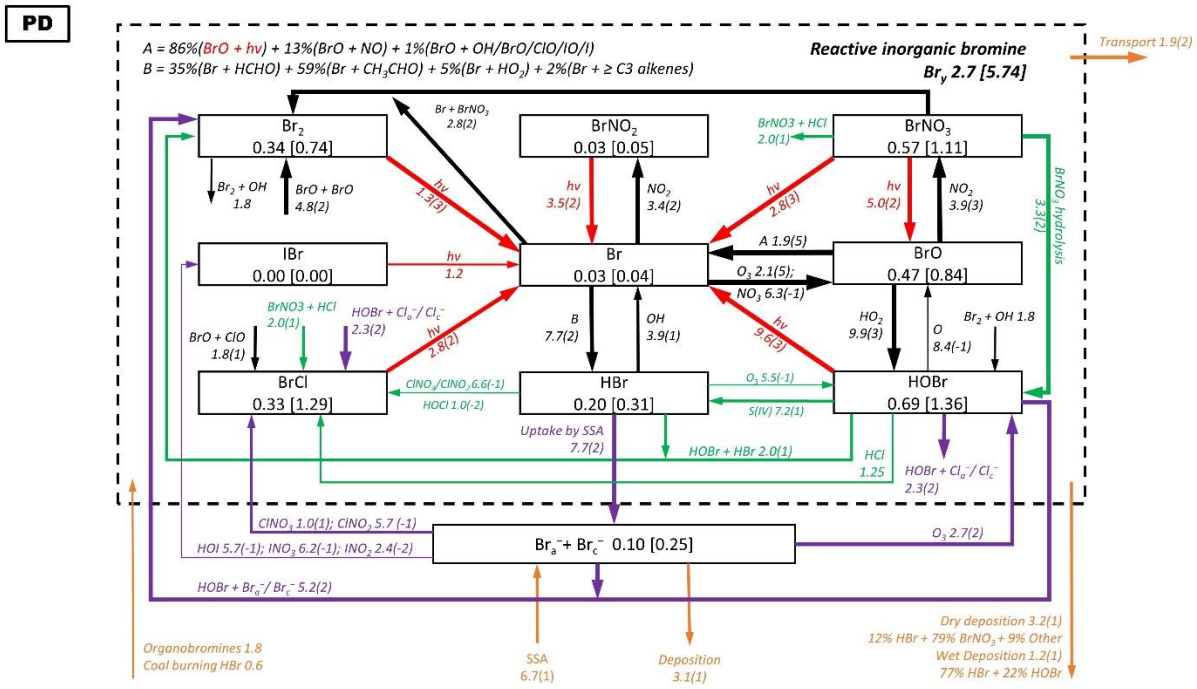

Figure S3. Similar to Figure S1 but for PD.

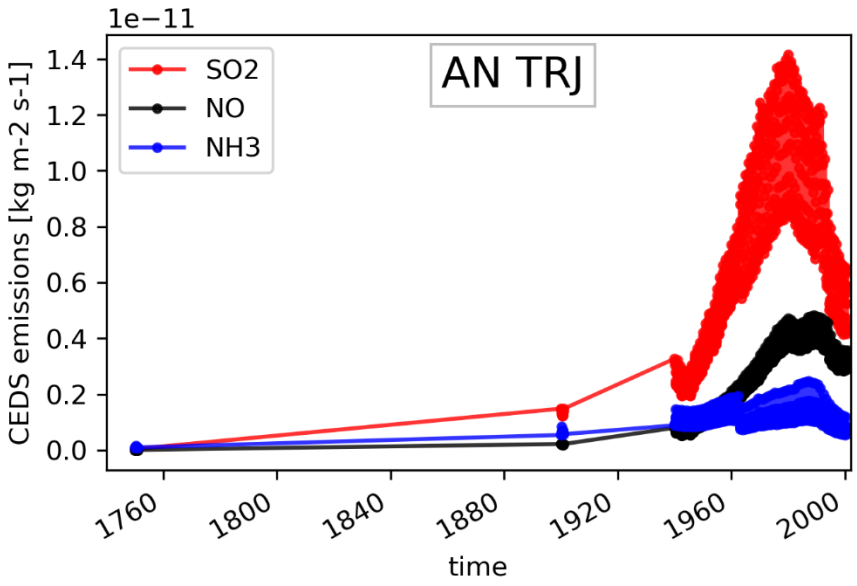

Figure S4 Anthropogenic SO_2, NO, and NH_3 emissions in hourly resolution from the Community Emissions Data System (CEDS) (Hoesly et al., 2018) in the AN TRJ. Note that only 1750, 1900, and post-1940 data are shown.

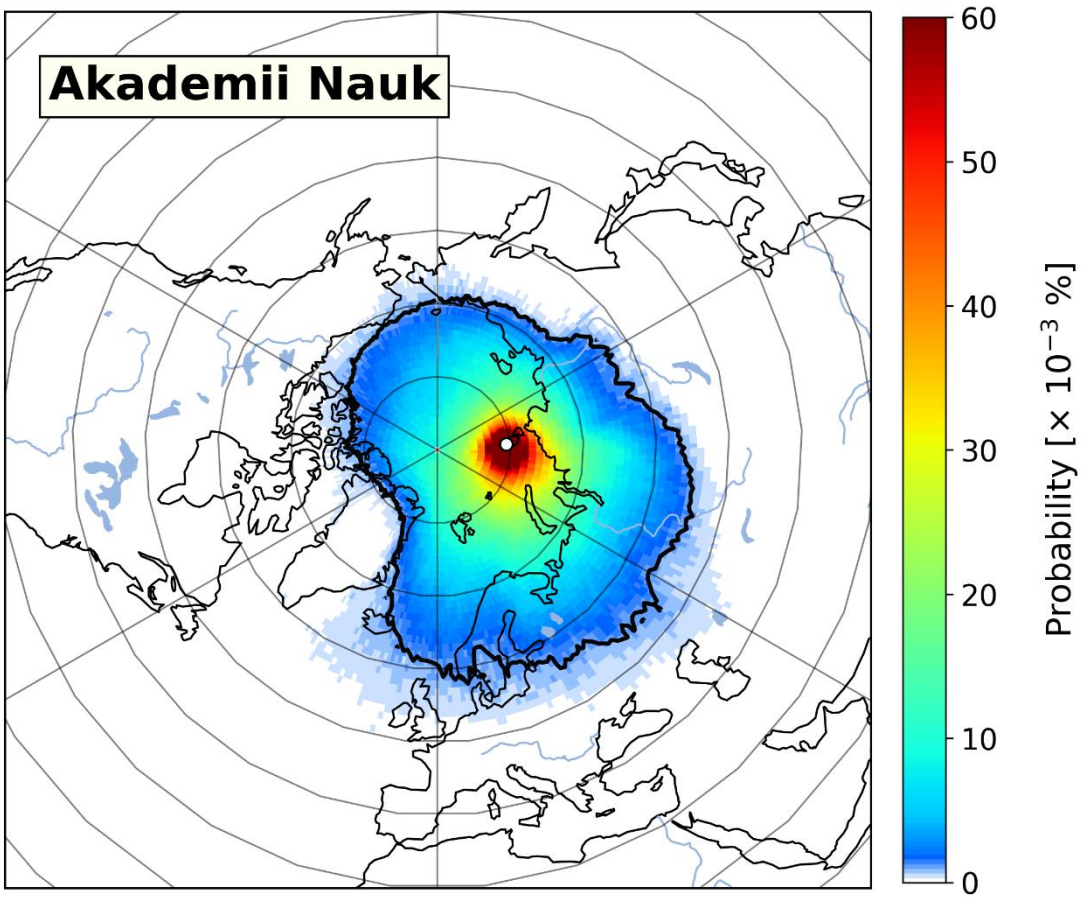

Figure S5 5-day back trajectory probability of AN calculated by the HYSPLIT model for the time period 1959-2010. The AN site is marked as a white circle, and the black contour indicate the TRJ (probability > 1.2×10^{-3} %) used for bromine budget analysis. Details of HYSPLIT model simulations can be found in Zhai et al., (2021)

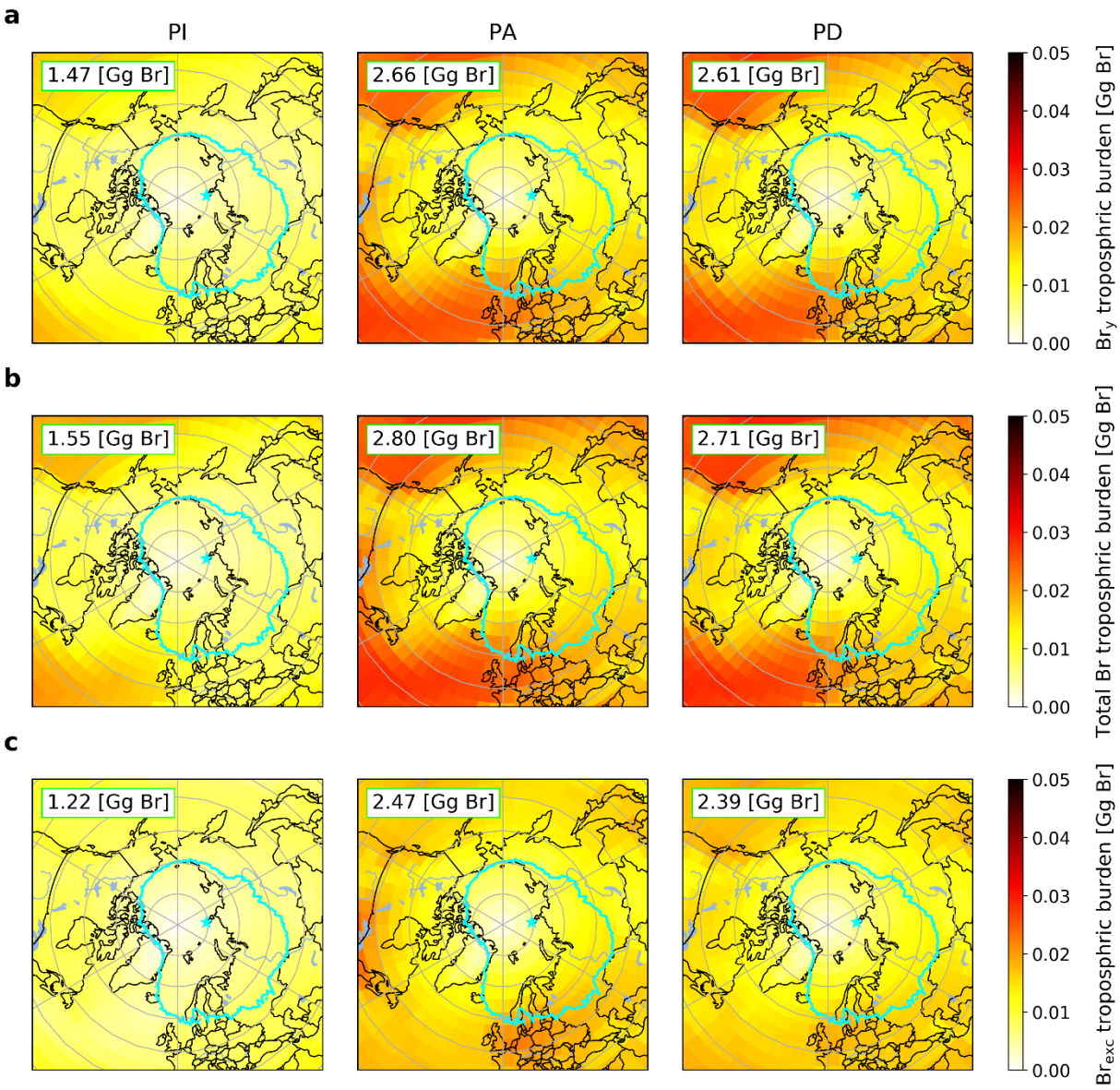

Figure S6 Regional distributions of annual mean tropospheric burden of a) Br_y b) total Br and c) Br_{exc} in the pre-industrial (PI = 1850), peak-acidity (PA = 1975), and present day (PD = 1999) simulated by GEOS-Chem. Gray grid lines show 10° latitude and 60° longitude distance, cyan star marks the AN ice-core location, and cyan lines show the 5-day TRJ for AN simulated by the HYSPLIT model (Fig.S5). Numbers on the top-left corners in are the annual mean tropospheric a) Br_y b) total Br and c) Br_{exc} burdens in the AN TRJ for the three time periods.

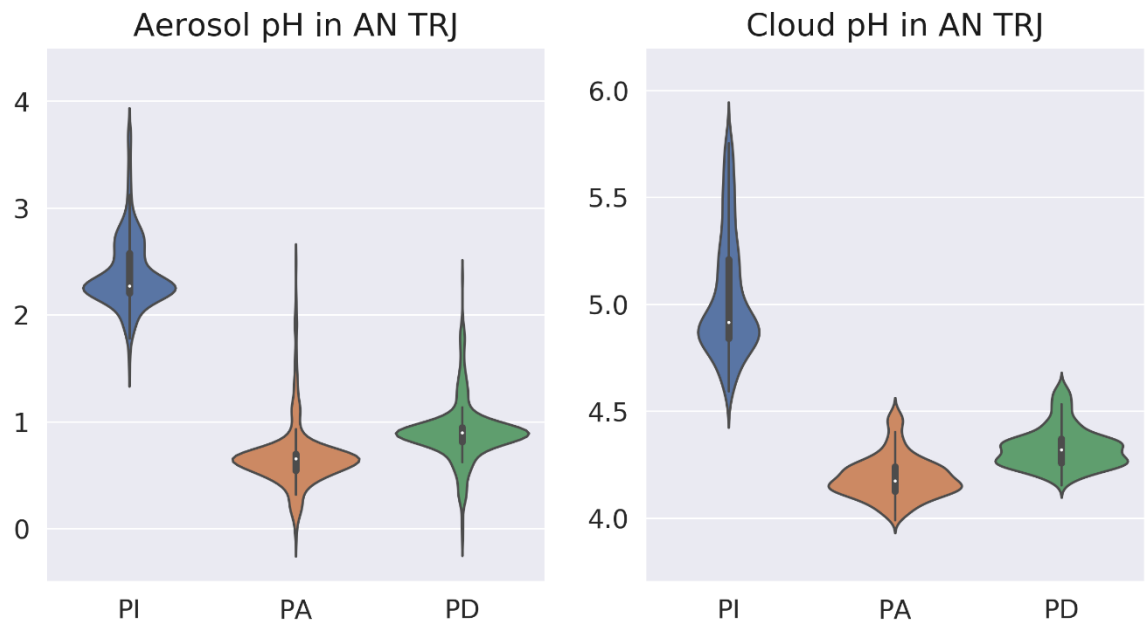

Figure S7 Violin plots of modeled annual mean left panel) aerosol pH and right panel) cloud pH in the AN TRJ for PI, PA, PD. Boxes in each violin plot shows the interquartile range (IQR, from first quartile to third quartile), and white dots show median. Thin lines show the range of 1.5×IQR of the data, and violins show the density, with widths representing the frequency of data. The mean of aerosol pH in the AN TRJ for PI, PA, PD are 2.39, 0.66, 0.90, respectively. The mean of cloud pH in the TRJ for PI, PA, PD are 4.98, 4.19, 4.33, respectively

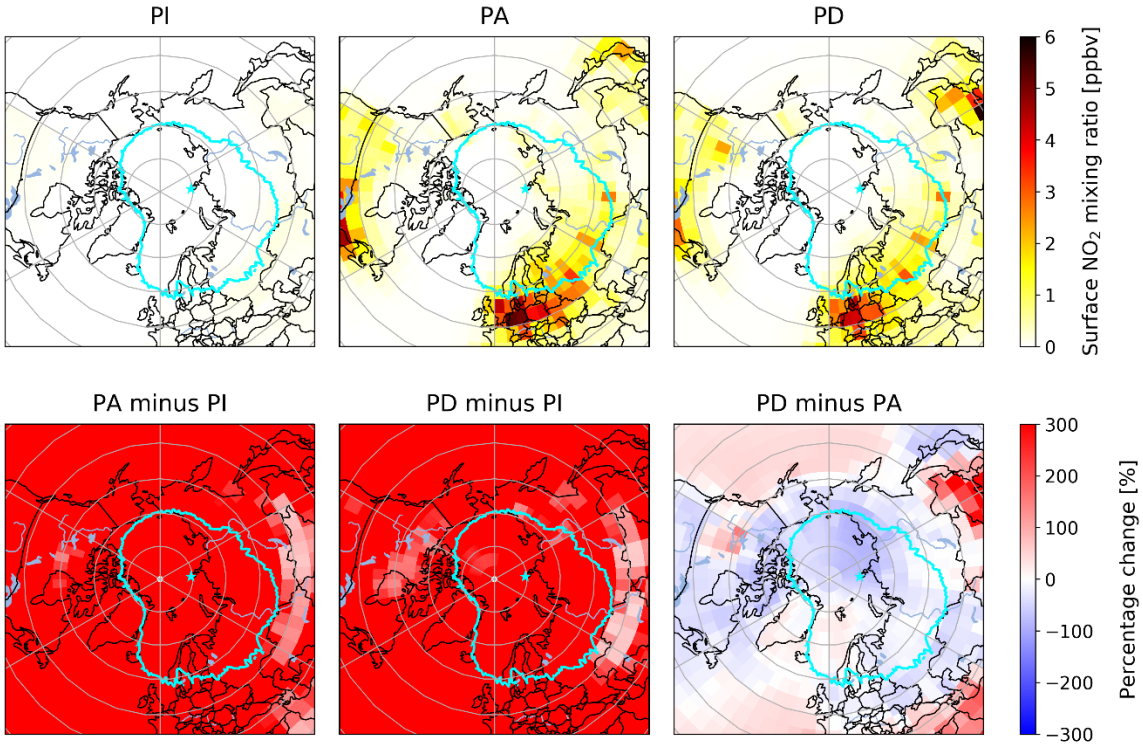

Figure S8 (Upper panels) Modeled NO_2 surface mixing ratios in PI, PA, and PD and (Lower panels) their percentage changes in between the three time periods. Cyan star and lines show the location of AN ice core and its 5-day TRJ.

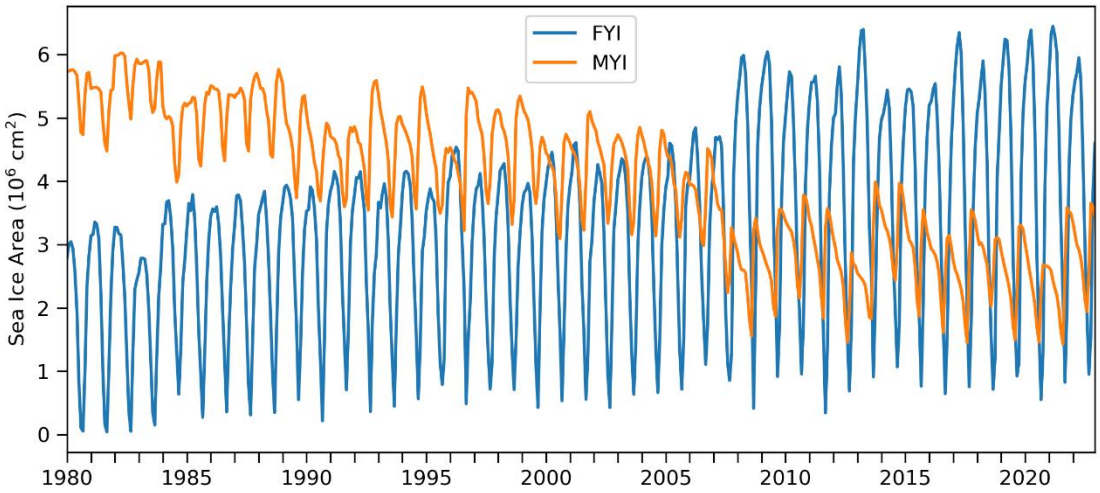

Figure S9 FYI and MYI trends in AN TRJ since 1980 based on Confer et al., 2023. FYI and MYI data are based on EASE-Grid Sea Ice Age for years after year 1984. Prior to year 1984 sea ice age is not available from observations, so MYI is based on the minimum sea ice extent in MERRA-2 at the end of summer. Annual average of FYI area are 1.96×10^6 cm^2 and 3.38×10^6 cm^2 in 1980 and 2007, respectively.

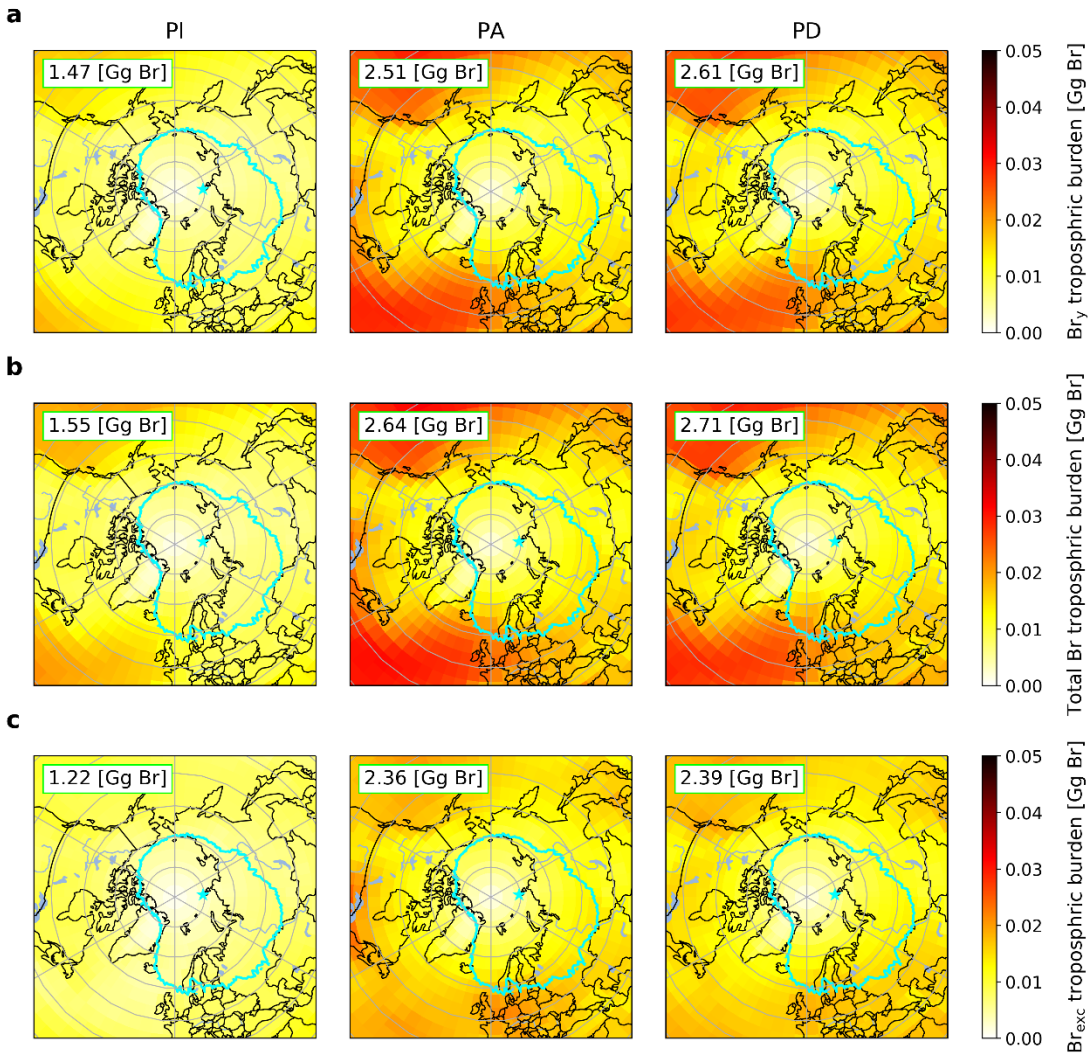

Figure S10 Similar to Figure S4 but for PA with 1980 (instead of 2007) meteorology.

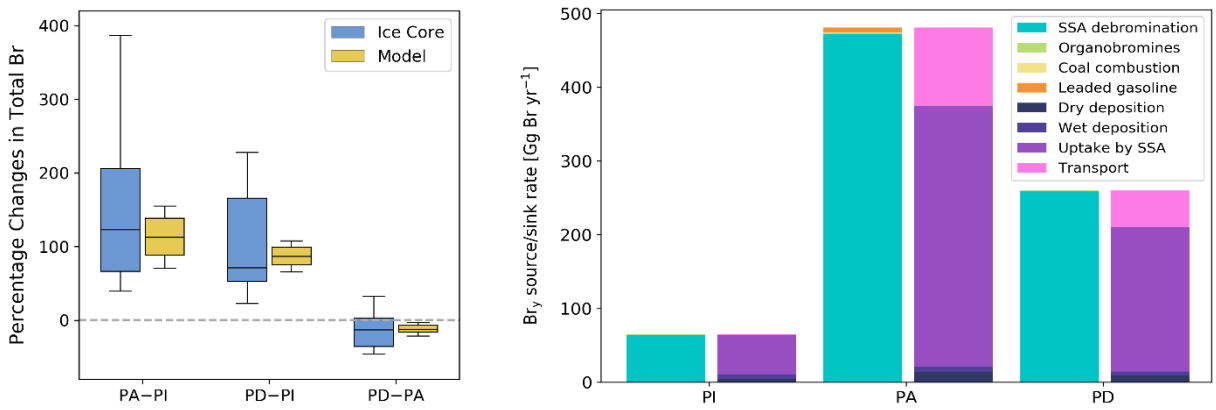

Figure S11 (left panel) Comparison of percentage changes in annual mean tropospheric total Br burdens between PI, PA, and PD from the Col du Dome (CDD) ice-core records and model simulations, and (right panel) modeled annual mean sources and sinks of tropospheric Br_y in the CDD TRJ for PI, PA, PD. For each time period, left bar shows the sources and right bar shows the sinks. 'SSA' is short for sea-salt-aerosol, and 'Transport' represents Br_y that transported outside of the CDD TRJ.

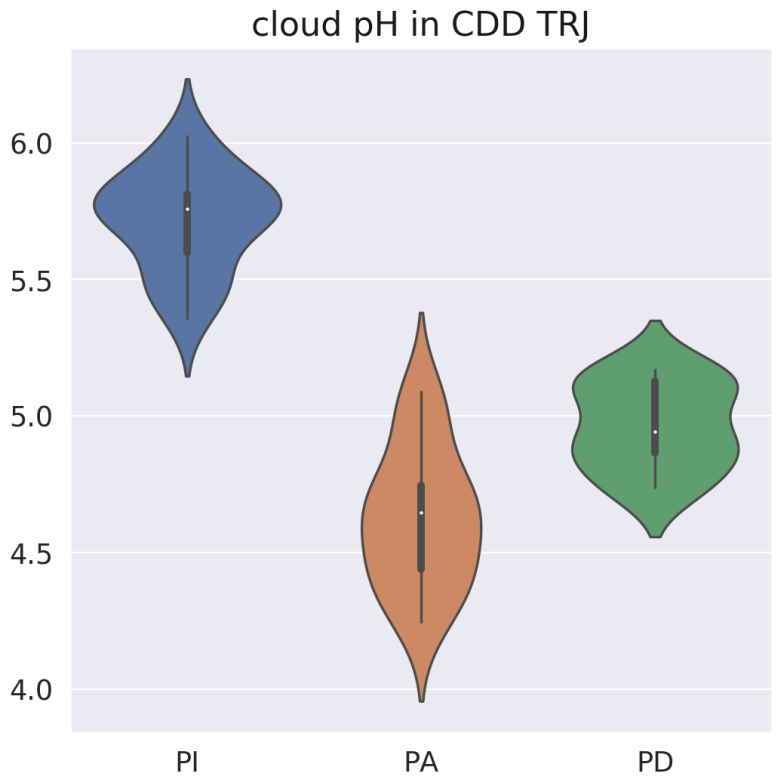

Figure S12 Violin plots of modeled annual mean cloud pH in the CDD TRJ for PI, PA, PD. Boxes in each violin plot shows the IQR, and white dots show median. Thin lines show the range of 1.5×IQR of the data, and violins show data density, with widths representing the frequency of data. The mean of cloud pH in the CDD TRJ for PI, PA, PD are 5.7, 4.6, 5.0, respectively.

Table S1 Bromine burden from leaded gasoline and coal combustion in the AN 5-day back-trajectory region for PI, PA, and PD, with corresponding global burdens shown in the brackets.

Burden (Gg Br)	Leaded gasoline		Coal combustion
	PbBrCl	CH_3Br	HBr
PI	–	–	0.00 (0.09)
PA	2.64 (113.33)	0.47 (23.75)	1.25 (23.63)
PD	–	–	0.62 (22.90)

Table S2 Average ice-core concentrations of nssNa, total Br, Br_{exc}, and acidity at AN over different time periods.

Ice-core concentrations	nssNa (ng g^{-1})	Total Br (ng g^{-1})	Br_{exc} (ng g^{-1})	Acidity (μM)	Br_{exc}/Br
1750–1850	98.18±59.12	2.02±0.88	1.41±0.71	2.16±1.93	69%±11%
1750–1940	140.06±135.04	2.40±1.45	1.53±0.81	2.17±1.83	65%±12%
1970–1980	219.27±136.48	7.06±4.05	5.71±3.34	11.81±5.39	80%±6%
1988–1998	153.87±76.6	3.32±1.14	2.36±0.89	3.34±2.26	70%±11%

Note: Calculated from raw ice-core data, including years with volcanic activities.

Table S3 Annual mean tropospheric bromine burden and speciation in the AN TRJ for PI, PA, and PD from model simulations

Burden (Gg Br)	Br_2	Br	BrO	HOBr	HBr	$BrNO_2$
PI	0.358	0.032	0.381	0.303	0.150	0.002
PA	0.350	0.028	0.444	0.681	0.213	0.041
PD	0.345	0.029	0.465	0.676	0.201	0.027

(Continued)

Burden (Gg Br)	$BrNO_3$	IBr	BrCl	Br_a^-	Br_c^-	Br_{exc}
PI	0.120	0.000	0.122	0.040	0.044	1.221
PA	0.590	0.000	0.315	0.111	0.026	2.472
PD	0.551	0.000	0.316	0.078	0.026	2.389